12-28-2018

Transient transmission oscillations in doped and undoped lithium niobate induced by near-infrared femtosecond pulses

Bryan J. Crossman
College of Saint Benedict/Saint John's University, bjcrossman@csbsju.edu

Gregory J. Taft
College of Saint Benedict/Saint John's University, gtaft@csbsju.edu

Recommended Citation

Transient Transmission Oscillations in Doped and Undoped Lithium Niobate Induced by Near-Infrared Femtosecond Pulses

Bryan J. Crossman - Email: bjcrossman@csbsju.edu

Gregory J. Taft[*]**- Email: gtaft@csbsju.edu**

Department of Physics, College of St. Benedict/St. John's University
2850 Abbey Plaza, Collegeville, MN 56321
[*] Corresponding author

Abstract

Transient transmission oscillations in X-cut and Z-cut congruent, iron-doped, and magnesium-doped lithium niobate samples were measured using 50-fs, 800-nm, 0.5-nJ pulses from a self-modelocked Ti:sapphire laser in an optical pump-probe system. Several Raman-active oscillation modes excited by these pulses were observed as changes in the transmitted probe intensity versus time delay between the pump and probe pulses. The samples were rotated to determine how the incident polarization of the pump pulses affects the mode excitations. The observed Raman-active oscillations correspond to previously reported symmetry modes measured with traditional, continuous-wave, Raman spectroscopy using the same scattering geometry. In addition, a polariton mode and other, previously unreported, lower-frequency modes were observed in each of the samples. The transmission intensity data for each sample were fit successfully to a superposition of sinusoidal functions with exponentially decaying amplitudes.

Introduction

Lithium niobate ($LiNbO_3$) is a ferroelectric material with interesting nonlinear optical, electro-optic, and piezoelectric properties that allow for applications in holographic memory storage, fast optical switching, and waveguide writing.[1-4] Because of the interest in utilizing lithium niobate in optical devices, it has been studied extensively with traditional continuous-wave (CW) Raman spectroscopy for different crystal cut orientations and incident light polarizations.[5-7] With the development of lasers capable of producing femtosecond pulses, suitably high electric field intensities and short pulse durations allowed for the possibility of making time-domain observations of coherent phonon oscillations in crystal lattices.[8-10] The coherent phonon oscillation modes are Raman-active, which lead to easy comparison with Raman spectra. Impulsive stimulated Raman scattering (ISRS) is a process in which a sufficiently high energy pump pulse stimulates these vibrational modes, which are then observed by sending a lower energy probe pulse into the excited sample at a controllable time delay after the pump pulse.[11] The pump-induced excitations in the sample can cause changes in the amount of probe pulse energy transmitted through the sample or small rotations to the polarization of the transmitted probe pulse.[12] Both processes can lead to changes in the amount of detected probe energy. In general, multiple vibrational modes of different frequencies are excited simultaneously, causing a beating pattern in the time-resolved scans on the sub-picosecond timescale. By computing the Fourier transform of the temporal scan, one can reproduce a Raman spectrum for comparison with those found using traditional CW Raman spectroscopy. Unlike CW Raman spectroscopy, ISRS gives information on the decay times for the Raman modes.

The advent of ultrashort pulsed lasers has been essential to the advancement of waveguide writing in lithium niobate crystals. Due to the relatively high peak intensities of high energy femtosecond laser pulses and the photorefractive properties of lithium niobate, it is possible to write three-dimensional waveguides.[4] Recent studies have investigated the photorefractive effect in lithium niobate using high-energy femtosecond laser pulses with fluences at or above the optical damage threshold of the material.[13] Our study, however, deals with much lower fluences (~20 μJ/cm^2) which allows for the observation of Raman-active vibrational modes without permanent changes to the sample. Detailed measurements of the frequencies and corresponding lifetimes of these oscillations are needed to provide an understanding of the ultrafast transient behavior of lithium niobate, especially for applications involving femtosecond laser pulses.

Doping of lithium niobate with transition metals and other metals has been beneficial in creating holographically-stored data within crystals which are less likely to be changed by illumination.[14,15] Though there have been studies which use the time-resolved ISRS technique on doped lithium niobate samples, there has not been a study which compares the Raman-active modes of multiple doping types with identical experimental conditions. Lattice defect sites occupied by dopant atoms create other oscillation modes not present in congruent lithium niobate (CLN) samples. The oscillation wavenumbers should be consistent with previous CW Raman spectra of doped samples.[16] Since the doping of lithium niobate samples causes the intensity and decay time of the oscillations to change, detailed knowledge of these oscillations could lead to future improvements in holographic memory storage devices.[17] In this study we discuss the differences in the measured Raman oscillation modes of lithium niobate samples that

are doped with iron and magnesium (referred to as Fe:LN and Mg:LN, respectively). Also, we report on how doping affects the amplitude and decay time of each observed oscillation mode.

Experiment

We use a femtosecond pump-probe laser system to observe ISRS in various lithium niobate samples. The experimental setup is shown in Fig. 1 and is similar to the one used in previous ISRS work.[18] Laser pulses are produced using a home-built self-mode-locked Ti:sapphire laser pumped with 4.25W of output from a commercial, 532-nm, CW, solid-state laser. The bandwidth of the Ti:sapphire laser output is 25-nm full-width-at-half-maximum ranging from 790 nm to 815 nm. Although a broader bandwidth is possible from this laser, the narrower 25-nm bandwidth makes material dispersion compensation simpler and still enables sufficiently short pulse durations for this work. The average output power of the laser is 0.75 W with a repetition rate of 82 MHz corresponding to 9 nJ of pulse energy. A 50/50 beam splitter creates the separate pump and probe beams. Double-pass fused silica prism pairs compensate for the material dispersion of the optical components in the system. When optimized, pump and probe pulses with durations of approximately 50 fs, measured using a second-harmonic generation Frequency Resolved Optical Gating, (SHG FROG) device,[19] and nearly Gaussian temporal shape are incident on the samples.

Along the pump path, an acousto-optic modulator (AOM) modulates the pump beam with a frequency of 25 kHz and allows for simple control of the pump beam power, which typically is set at 40 mW. The probe beam power is controlled using a linear gradient filter. The probe power is maintained at 1 mW, which at only 2.5% of the pump power should have less effect on the sample. Both the pump and probe pulses overlap spatially and temporally at the surface of the

sample. Probe pulses that interact with sample material excited by the pump pulses also become modulated at 25 kHz, allowing for lock-in amplification detection. To ensure that no pump pulse energy is detected, pump pulses are polarized orthogonal to probe pulses using a half-wave plate and a vertical polarizer. A horizontal polarizer located in front of a silicon photodiode detector only lets through the horizontally-polarized probe pulses. This differs slightly from other ISRS setups in which the final polarizer transmission axis is oriented at a 45-degree angle to maximize detection of polarization rotation of the probe pulse. Since the polarizer transmission axis in our setup is oriented parallel to the linearly polarized probe pulses, polarization rotation cannot adequately explain the change in the detected probe pulse energy that we measure. As described below, our measurements suggest that the oscillations we observe are due to transient transmission changes and not polarization rotation.

A motorized translation stage with an attached retroreflecting mirror produces a time delay between the pump and probe pulses. The motor used, a Zaber Technologies model T-LA28A (Vancouver, Canada), has a step size of 0.1 μm corresponding to a minimum time delay step size of less than 1 fs. This enables the observation of both the initial nonlinear optical excitation and the subsequent Raman oscillations in the samples. Each sample is placed on a stage composed of two orthogonal, manual, linear translation stages to control the sample's position parallel to the optical table surface. The pump and probe pulses are incident on the sample at angles of 10 degrees and 20 degrees, respectively. The pump and probe beams are focused onto the sample with separate lenses (pump and probe lens focal lengths of 15 and 20 cm, respectively) with measured beam waist diameters of 60 μm and 20 μm, respectively. With this configuration the transmitted pump beam is blocked from reaching the detector. The cross-correlation of the pump

and probe pulses at the sample was measured (Fig. 2a) to have a full-width-at-half-maximum of 90 fs using a beta barium borate (BBO) second harmonic generation crystal with a thickness of 0.5 mm. This measurement was made by placing the BBO crystal at the normal sample location. The interaction between the pump and probe photons generating second harmonic light along the bisector of the two beams decreases the amount of probe light transmitted through the sample; thus, measurement of the cross-correlation shows a decrease in the transmitted probe intensity. Although the silicon photodiode detector is not sensitive to the second harmonic light, an optical filter was placed before the detector to prevent any second harmonic light from reaching the detector during the cross-correlation measurement.

The optical grade lithium niobate samples (both doped and undoped) purchased from MTI Corporation each has dimensions 10 mm x 10 mm x 0.5 mm. Two cut orientations (X-cut and Z-cut) of undoped lithium niobate are used in this experiment; all doped samples are Z-cut. The doping levels of the magnesium and iron doped samples are 5% mol and 0.07% mol, respectively.

In one part of this experiment, we investigate how the signal of the ISRS process is influenced by the direction of the pump pulse polarization with respect to the sample. Thus, for a Z-cut sample, measurements are taken using both X and Y polarization of the pump pulse by rotating the sample 90 degrees about the Z-cut face. The polarizations of the pump and probe pulses always are kept orthogonal to one another to prevent the detection of any scattered pump pulse energy.

Once the sample is in place, small adjustments are made to the final mirror in the pump path to optimize the spatial overlap of the two pulses. This is aided by using a computer-interfaced camera to observe a magnified image of the scattered light from the pump and probe

spots on the sample surface. Also, we make small adjustments to the spatial overlap to maximize the lock-in amplifier signal during the nonlinear excitation that occurs at zero time delay. A computer program controls the motion of the stepper motor and acquires a voltage reading from the lock-in amplifier, which receives a 25-kHz reference signal from the AOM driver. To further minimize noise, a pre-amplifier filters out signals with frequencies outside of the 10-30 kHz range.

For the measurements reported in this work, the lock-in amplifier was set to detect changes in voltage from the photodiode detector of less than 3 μV. The average signal detected from the nonlinear excitation was less than 1 μV. The measured oscillations have an average amplitude of about 0.05 μV. With the average noise of the system around 0.003 μV, the signal to noise ratio of the system is above 16 to 1. Each of the scans shown in this manuscript are averages of four sequential scans using the same sample in the same orientation. All scans have a time delay step size of 5 fs between the measured signal values. Uncertainty in the measured signal values is estimated by calculating the standard deviation of the signal values for each of the 4 sequential scans at each time delay.

We compute the fast Fourier transform (FFT) of the scan data to observe the coherent oscillations in the spectral domain. So that we can focus on the oscillations, we exclude the first part of the scan up to a time delay of 120 fs. Before computing each FFT, the scan data with a range of 5 ps is padded with zeros for a total range of 10 ps. This decreases the FFT output spacing to 2 cm^{-1}. Based on this and comparison of the wavenumbers of the peaks in the FFTs of repeated scans, the uncertainty in the wavenumber of the peaks is estimated to be ± 1 cm^{-1}.

Results

When doing a pump-probe experiment of this type, it is important to know the duration of time when the pump and probe pulses are both present in the sample simultaneously. This often is the limiting factor determining which oscillation modes are observable, since the interaction (or cross-correlation) time must be shorter than the oscillation period in order to produce coherent phonons in the sample. The measured cross-correlation is shown in Fig. 2a accompanied with a typical scan in Fig. 2b of the Z-cut CLN sample with X pump polarization. During the initial ~100-fs interaction time of the pump and probe pulses in the sample, the probe light transmitted through the sample drops slightly below the equilibrium value and then increases significantly higher before returning close to the equilibrium value. With our setup any polarization rotation of the probe beam would cause a *decrease* in the transmission, since the polarizer before the detector is oriented to maximize the transmission of the horizontally-polarized probe light. Therefore, we rule out polarization rotation as an explanation for the increase in the transmission. Also, this initial excitation is not due to linear absorption in the lithium niobate, since the bandgap energy is ~4eV and the pump photon energy is only ~1.5 eV. Even two-photon absorption is unlikely for our pump pulse wavelength as shown by Byer *et al*.[20] Although the exact nonlinear process responsible for the initial excitation is unknown, it appears to create sufficient off-resonant excitation necessary for the ISRS technique. In our work we focus on the oscillations in the transmitted probe light observed after the initial nonlinear excitation; therefore, the scans presented in the rest of this manuscript start ~120 fs after the peak of the initial nonlinear excitation, enabling the oscillations to be seen more clearly.

As a verification of our experimental setup, ISRS measurements of congruent lithium *tantalate* (CLT) made with our system compare well with similar measurements made by Hu *et al.*[21] Figs. 3a and 3b show the scans and FFTs of CLT with the pump beam polarized in both the X and Y directions. Our FFT reveals Raman-active oscillation modes at wavenumbers of 202, 356, 371, and 456 cm^{-1}. Except for the large peak in the CLT FFT at 371 cm^{-1}, the wavenumbers of the peaks agree with those determined by Hu *et al.*[21] The 371 cm^{-1} peak that does not match a previously reported Raman wavenumber may be a polariton mode like we observed in the lithium niobate samples described below.

We also examined how the average power of the pump beam affects the peak intensities of the Raman-active oscillation modes. The Z-cut CLN sample was placed with the pump beam polarized in the X direction of the crystal, and the average power of the pump beam was changed between the scans. The probe power was adjusted to keep it at less than 10% of the total pump power. The results of the calculated FFTs for each scan are shown in Fig. 4a. As expected, there is an increase in the FFT intensity with increasing average pump power. Fig. 4b shows the maximum FFT intensity of each scan, which occurs at a wavenumber of ~300 cm^{-1}. The plot of average power versus maximum FFT intensity follows a linear relationship (fit shown in figure). In stimulated Raman scattering experiments, it is expected that the intensity of these peaks will increase linearly with respect to increasing electric field intensity.[21,22] Because our measurements confirm this linear relationship, it is likely that the observed oscillations are due to the production of coherent phonons in the lithium niobate samples and not some other phenomenon. For the remaining scans, the pump power was held constant at 40 mW.

The Z-cut CLN was rotated to determine how the pump polarization direction affects the Raman modes observed in the scans. Fig. 5a shows the scans taken from the Z-cut CLN with 0, 45, and 90-degree pump polarization directions with respect to the X-axis of the sample. The accompanying FFTs of these scans are shown in Fig. 5b. The FFTs show consistency between the 0 and 90-degree scans both in the intensity of the peaks and the wavenumbers at which they occur. For the 45-degree pump polarization, however, an oscillation mode at 240 cm^{-1} appears that is not apparent in either of the other scans. Also, there are significant changes in the intensities of the FFT peaks. Thus, by changing the polarization direction of the pump beam relative to the crystal axes, we can excite some oscillations more than others.

In the scans for the X-cut CLN samples (shown in Fig. 6a), we observe dominant oscillations with a period of approximately 2 ps. This appears in the FFTs in Fig. 6b as the 23 cm^{-1} wavenumber peaks that are significantly stronger than the higher wavenumber peaks barely visible on these figures. For Y-polarization of the pump beam, there are three other modes observable in the FFT at wavenumbers of 266, 275, and 334 cm^{-1}. Only one higher wavenumber FFT peak is visible with the pump polarized in the Z direction at 275 cm^{-1}; however, the scaling on the Y-axis of Fig. 6b shows that these modes in both scans appear with amplitudes much smaller than the low wavenumber modes.

Fig. 7a shows scans of the Z-cut lithium niobate samples that are undoped (CLN), doped with iron (Fe:LN), or doped with magnesium (Mg:LN). Each of the scans shown were taken with the pump beam polarized in the X direction. The scans of CLN and Fe:LN have a very similar oscillation pattern, and the FFTs in Fig. 7b reveal that the oscillation modes excited in these two samples are identical. CLN has oscillation modes with wavenumbers 16, 23, 279, 300, and 333

cm^{-1}; whereas, Fe:LN has modes occurring at 17, 278, 300, and 332 cm^{-1} with an uncertainty of ± 1 cm^{-1}. Although there is no difference in the oscillation frequencies of these two samples, the amplitudes of these oscillations are somewhat larger for the Fe:LN sample under identical experimental conditions. The Mg:LN sample has an oscillation mode at a wavenumber of 240 cm^{-1} that is not apparent in either the Fe:LN or the CLN scans. Also, the peaks of the FFT have smaller amplitudes than those for either the Fe:LN or CLN.

Discussion

The Raman-active oscillation modes we observed through our ISRS study were compared with CW Raman spectra with the same scattering geometry.[5,6] We observed oscillations with wavenumbers of 275 and 334 cm^{-1} in the X-cut CLN FFTs, which match within uncertainty the wavenumbers associated with the transverse optical modes identified in previous work at 274 cm^{-1} [2A$_1$(TO)] and 334 cm^{-1} [3A$_1$(TO)].[5] The Z-cut CLN FFTs show similar modes at wavenumbers of 276 and 332 cm^{-1}, which are consistent with the previously identified longitudinal optical mode wavenumbers 276 cm^{-1} [1A$_1$(LO)] and 334 cm^{-1} [2A$_1$(LO)].[5,6] The FFTs contain another mode at 300 cm^{-1} which matches the wavenumber of the previously identified polariton wave in the crystal. This is a dispersive effect that occurs at low scattering angles.[5] In the case of the Mg:LN sample, there is an active vibrational mode which occurs at 240 cm^{-1} due to stimulation of the transverse optical 2E(TO) Raman mode identified at this wavenumber in CW Raman measurements.[5] Oscillations with wavenumbers of less than 50 cm^{-1} are not attributed to Raman modes in previous research, but could be acoustic phonons excited from the initial nonlinear impulse.

The most intense peaks in the FFTs for each scan were used to develop a theoretical fitting function for the temporal scans. The function is a linear combination of the various oscillations with exponentially decaying amplitudes described mathematically as:

$$\Delta T/T = \sum_{n=1}^{N} a_n \exp[(t - t_0)/\tau_n] \sin[2\pi c k_n t + \varphi_n]$$

where N is the number of visible oscillation modes from the FFT, a_n is the oscillation amplitude, t is the time delay of the probe relative to the time, t_0, at which the nonlinear interaction peaks, τ_n is the decay time, k_n is the wavenumber of the oscillation, c is the speed of light, and φ_n is the phase of each mode. This function successfully models the behavior of all but one of the lithium niobate scans. Only the X-cut sample with the pump polarized in the Z-direction requires the slightly-modified function:

$$\Delta T/T = a_0 \exp[(t - t_0)/\tau_0] + \sum_{n=1}^{N} a_n \exp[(t - t_0)/\tau_n] \sin[2\pi c k_n t + \varphi_n]$$

where the extra term in front of the summation represents a non-oscillating, exponentially decaying process with a decay time of 190 fs. This may indicate a relaxation from the nonlinear interaction instead of another Raman-active oscillation mode.

An example fit is shown in Fig. 8 for the Z-cut CLN scan with the pump beam polarized in the X-direction. Fit parameters for each of the Z-cut scans are shown in Table I and those for the X-cut scans in Table II. Small differences between the wavenumbers of the peaks in the FFT and the fit parameters can be attributed to the uncertainty from the Fourier transforms discussed above. Fit accuracy is determined by calculating the reduced chi-squared (χ^2) values as shown in Tables I and II. Some of the χ^2 values are slightly larger than one because the fits do not account

for small long-term variations in the background noise towards the end of some scans. The X-cut CLN scan with the pump polarization in the Y-direction was fit to the first of the two fitting functions using five wavenumbers; however, a successful fit required three low wavenumber modes compared to the Z-cut scans that required only one or two low wavenumber modes.

The amplitudes of the oscillations in the fit and of the peaks in the FFTs show which modes were most excited in a certain orientation. As for the oscillation modes visible in the CLN and Fe:LN samples, the amplitudes of the modes change in a similar manner when going between the X and Y pump polarization directions. Specifically, the amplitudes a_1 and a_4 are largest for the X polarization, while a_3 and a_5 are largest for the Y polarization. The situation is different with the Mg:LN sample, which has a larger amplitude a_2 for the X polarization and larger amplitudes a_1, a_4, and a_5 for the Y polarization. The amplitude a_3 is almost the same for both polarizations. This different behavior for Mg:LN likely is due to the higher doping (5%) compared to the Fe:LN (0.07%).

Just as the oscillation amplitudes are affected by the change in polarization, the decay times of the Raman-active modes also are affected. Essentially the decay times quantify how long it takes for each phonon to lose its energy to other undetected modes. One of the most notable changes in decay time with polarization direction is τ_3, which is longest for the X pump polarization in both the CLN and Fe:LN samples. However, this change in time delay is much less pronounced in the Mg:LN sample. Another interesting aspect of this data set is the decay time τ_2 for the 2E(TO) mode in Mg:LN, which is 30% larger for the Y polarization than for the X polarization. Also, it is significantly longer than any of the other decay times. Because the E-mode

oscillations are doubly degenerate, we expect to see a longer decay time than the singly degenerate A modes.

Summary

We used the ISRS technique to observe transient transmission oscillations on the sub-picosecond level due to the excitation of Raman-active coherent phonon modes in lithium niobate crystals. We observed oscillations primarily of symmetry modes $1A_1(LO)$ and $2A_1(LO)$ in both doped and undoped LN Z-cut samples and modes $2A_1(TO)$ and $3A_1(TO)$ for X-cut samples. Also, we were able to observe and identify a polariton wave oscillation mode, and low wavenumber oscillations that have not been attributed previously to specific symmetry modes. Lastly, we saw stimulation of the $2E(TO)$ mode in the Mg:LN Z-cut sample. Fits were applied to each Z-cut and X-cut scan using a superposition of damped sinusoidal oscillations. Amplitudes and relaxation times were determined using these fits. We made comparisons between the fit parameters of doped and undoped LN crystals to see how doping affects the observed oscillation modes, their amplitudes, and their decay times.

Acknowledgements

References

1. R. S. Weis and T. K. Gaylord: Lithium Niobate: Summary of Physical Properties and Crystal Structure. *Appl. Phys. A*, **37**, 191 (1985).

2. A. Yariv, S. S. Orlov, and G. A. Rakuljic: Holographic storage dynamics in lithium niobate: theory and experiment. *J. Opt. Soc. Am. B,* **13**, 2513 (1996).

3. R. Mankowsky, A. von Hoegen, M. Först, and A. Cavalleri: Ultrafast Reversal of the Ferroelectric Polarization. *Phys. Rev. Lett.*, **118**, 197601 (2017).

4. R. R. Thomson, S. Campbell, I. J. Blewett, A. K. Kar, and D. T. Reid: Optical waveguide fabrication in *z*-cut lithium niobate (LiNbO3) using femtosecond pulses in the low repetition rate regime. *Appl. Phys. Lett.,* **88**, 111109 (2006).

5. V. S. Gorelik and P. P. Sverbil: Raman Scattering by Longitudinal and Transverse Optical Vibrations in Lithium Niobate Single Crystals. *Inorganic Materials,* **51**, 1104 (2015).

6. R. F. Schauzele and M. J. Weber: Raman Scattering by Lithium Niobate. *Physical Review*, **152**, 705 (1966).

7. Y. Zhang, L. Guilbert, P. Bourson, K. Polgár and M. D. Fontana: Characterization of short-range heterogeneities in sub-congruent lithium niobate by micro-Raman spectroscopy. *J. Phys.: Condens. Matter,* **18**, 957 (2006).

8. Y. Ikegaya, H. Sakaibara, Y. Minami, I. Katayama, and J. Takeda: Real-time observation of phonon-polariton dynamics in ferroelectric LiNbO3 in time- frequency space. *Appl. Phys. Lett.,* **107**, 062901 (2015).

9. P. C. M. Planken, L. D. Noordam, T. M. Kermis, and A. Lagendijk: Femtosecond Time-Resolved Study of the Generation and Propagation of Phonon Polaritons in $LiNbO_3$. *Phys. Rev. B,* **45,** 7106 (1992).

10. V. S. Gorelik, O. G. Zolotukhin, T. V. Moskaleva, and M. M. SushchinskiT: Stimulated Raman scattering by transverse and longitudinal lattice vibrations in LiNbO3 and LiTaO3. *Sov. J. Quantum Electron.,* **13,** 1300 (1983).

11. L. Dhar, J. A. Rogers, and K. A. Nelson: Time-Resolved Vibrational Spectroscopy in the Impulsive Limit. *Chem. Rev.,* **94**, 157 (1994).

12. D. Turchinovich, P. Uhd Jepsen, B. S. Monozon, M. Koch, S. Lahmann, U. Rossow, and A. Hangleiter: Ultrafast polarization dynamics in biased quantum wells under strong femtosecond optical excitation. *Phys. Rev. B,* **68**, 241307 (2003).

13. O. Beyer, I. Breunig, F. Kalkum, and K. Buse: Photorefractive effect in iron-doped lithium niobate crystals induced by femtosecond pulses of 1.5 μm wavelength. *Appl. Phys. Lett*., **88**, 051120 (2006).

14. T. R.Volk, V. I. Pryalkin and N. M. Rubinina: Optical-damage-resistant LiNbO3:Zn crystal. *Opt. Lett.,* **15**, 996 (1990).

15. Y. Furukawa, K. Kitamura, Y. Ji, G. Montemezzani, M. Zgonik, C. Medrano, and P. Günter: Photorefractive properties of iron-doped stoichiometric lithium niobate. *Opt. Lett.*, **22**, 501 (1997).

16. R. Mouras, M. D. Fontana, P. Bourson, and A. V. Postnikov: Lattice site of Mg ion in LiNbO3 crystal determined by Raman spectroscopy. *J. Phys.: Condens. Matter,* **12**, 5053 (2000).

17. K. Buse, A. Adibi, and D. Psaltis: Non-volatile holographic storage in doubly doped lithium niobate crystals. *Nature*, **393**, 665 (1998).

18. G. J. Taft, M. T. Newby, J. J. Hrebik, M. Onellion, T. F. George, D. Szentesi, S. Szatmari, and L. Nanai: Ultrafast dynamic reflectivity of vanadium pentoxide. *J. Mater. Res.,* **23**(2), 308 (2008).

19. G. Taft, A. Rundquist, M. M. Murnane, H. C. Kapteyn, K. DeLong, R. Trebino, and I. Christov: Ultrafast optical waveform measurements using Frequency Resolved Optical Gating. *Opt. Lett.,* **20**, 743 (1995).

20. O. Beyer, D. Maxein, K. Buse, B. Sturman, H. T. Hsieh, and D. Psaltis: Femtosecond time-resolved absorption processes in lithium niobate crystals. *Opt. Lett.,* **30**, 1366 (2005).

21. J. Hu, O. V. Misochko, H. Takahashi, H. Koguchi, T. Eda, and K. G. Nakamura: Ultrafast zone-center coherent lattice dynamics in ferroelectric lithium tantalate. *Sci. Technol. Adv. Mater.,* **12**, 034409 (2011).

22. H. Sasaki, R. Tanaka, Y. Okano, F. Minami, Y. Kayanuma, Y. Shikano, and K. G. Nakamura: Coherent control theory and experiment of optical phonons in diamond. *Sci. Rep.*, **8**, 9609 (2018).

Table I. Fit parameters used to reproduce the dynamic transmission data for all Z-cut scans using both X and Y pump polarizations.

Sample	Pump		2E(TO)	1A$_1$(LO)	Polariton	2A$_1$(LO)	χ^2
				Amplitudes, A.U.			
		a_1	a_2	a_3	a_4	a_5	
CLN	X	0.084		0.042	0.095	0.069	3.69
	Y	0.046		0.150	0.061	0.099	1.60
Fe:LN	X	0.065		0.059	0.083	0.080	1.52
	Y	0.050		0.135	0.062	0.096	2.94
Mg:LN	X	0.051	0.024	0.141	0.029	0.125	2.73
	Y	0.075	0.009	0.138	0.043	0.141	2.95
				Wavenumbers, cm^{-1}			
		k_1	k_2	k_3	k_4	k_5	
CLN	X	21		273	298	333	
	Y	16		273	301	332	
Fe:LN	X	16		273	300	332	
	Y	18		274	301	332	
Mg:LN	X	17	239	274	302	331	
	Y	16	240	275	299	332	
				Decay Times, fs			
		τ_1	τ_2	τ_3	τ_4	τ_5	
CLN	X	635		793	786	886	
	Y	937		373	892	691	
Fe:LN	X	680		635	853	800	
	Y	933		410	882	723	
Mg:LN	X	932	1978	494	896	747	
	Y	878	2572	437	1011	532	

Table II. Fit parameters used to reproduce the dynamic transmission data for the X-cut CLN scans using both X and Y pump polarizations

Pump					2A$_1$(TO)	3A$_1$(TO)	χ^2
			Amplitudes, A.U.				
	a_0	a_1	a_2	a_3	a_4	a_5	
X		0.014	0.113	0.009	0.023	0.014	0.44
Y	0.33		0.212		0.052		0.78
			Wavenumbers, cm^{-1}				
	k_1	k_2	k_3	k_4	k_5		
X	8	25	42	275	333		
Y		22		277			
			Decay Times, fs				
	τ_1	τ_2	τ_3	τ_4	τ_5		
X	2793	843	1548	575	949		
Y	190	628		629			
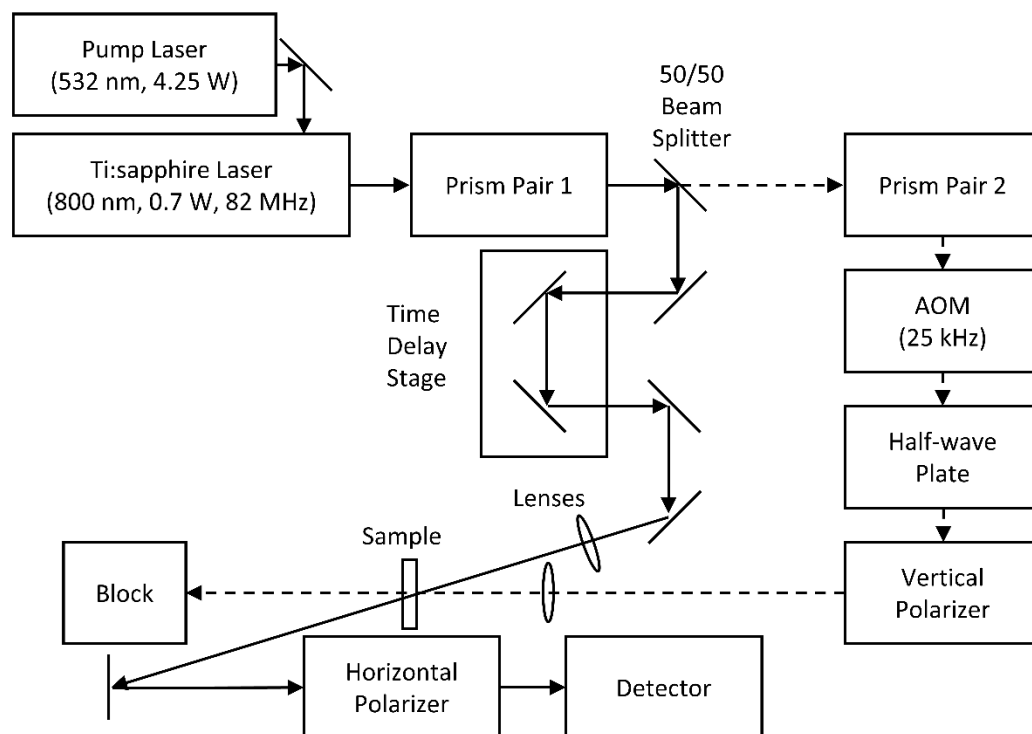
FIG 1. Diagram of pump-probe system

(a)

(b)
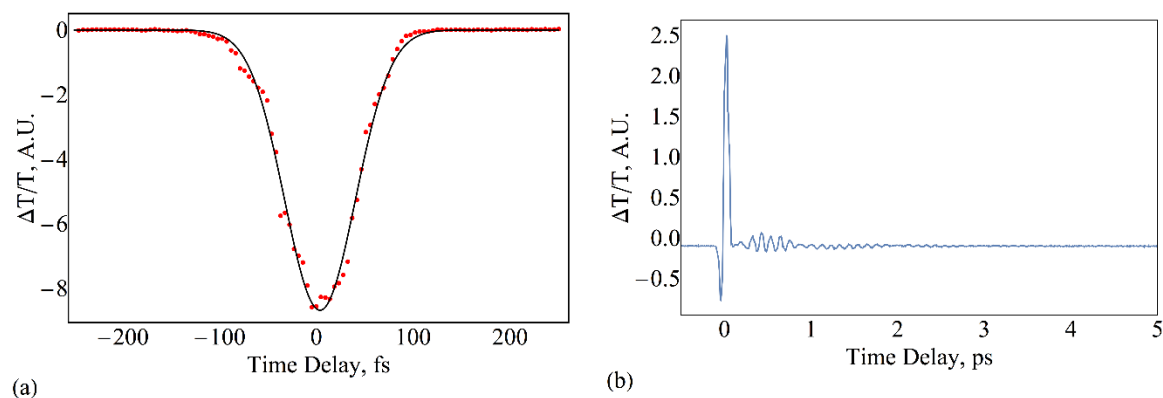
FIG 2. Experimental determination of interaction between pump and probe pulses (cross-correlation) in the sample: (a) measured cross correlation using a second harmonic generation crystal and (b) full scan of transmitted probe light using a Z-cut CLN crystal showing the large nonlinear signal occurring only when the pump and probe pulses are both in the sample.
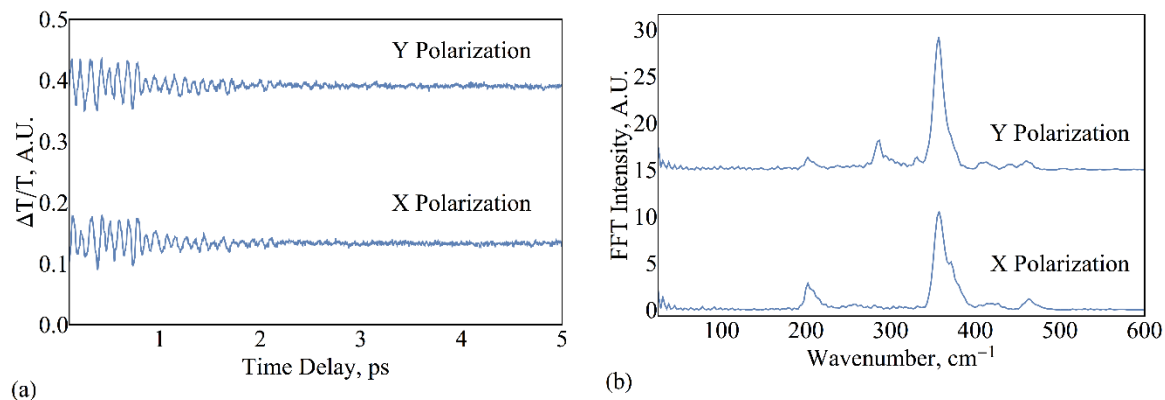
FIG 3. (a) Scan data taken for Z-cut CLT with pump polarization in both the X and Y directions and (b) accompanying FFT for each of the scans.
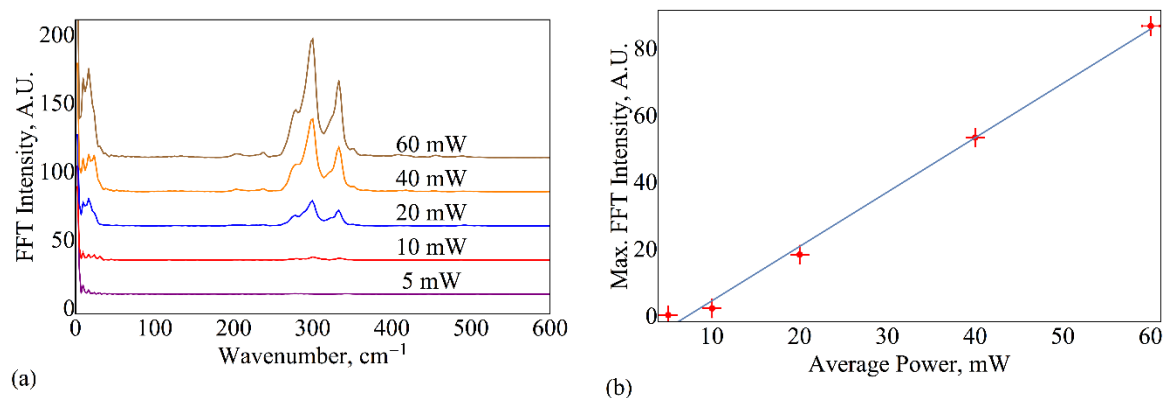
FIG 4. Increasing the average pump power causes a proportional change in the FFT maximum intensity. The plots show (a) FFTs of transmission scans using the Z-cut CLN with X pump polarization with varying power and (b) a linear fit of maximum FFT intensity versus average pump power.
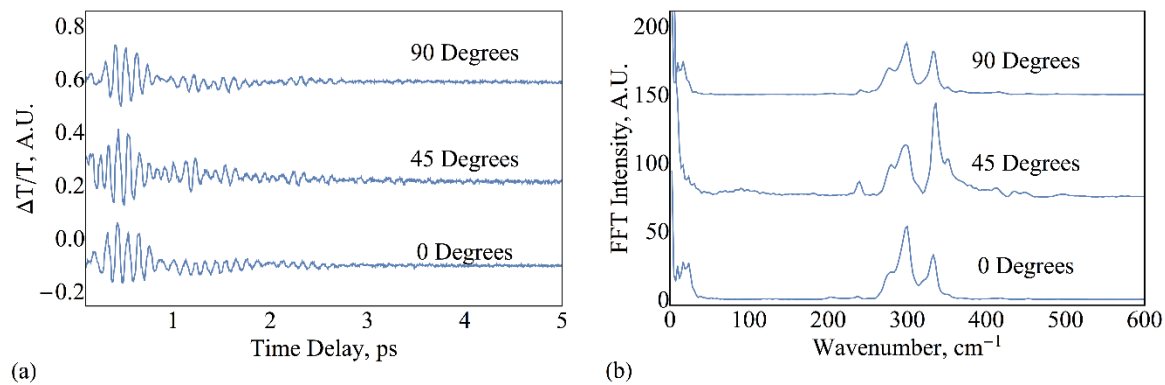
FIG 5. Observation of how the (a) scans and (b) corresponding FFTs change when rotating the
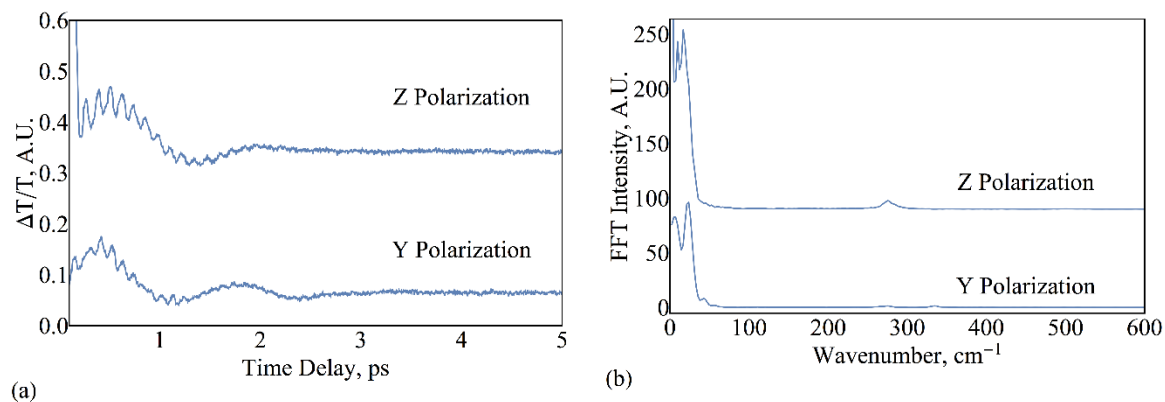
CLN sample about the Z-cut face.

FIG 6. (a) Transmission scans of X-cut CLN samples using both polarizations of pump pulses and
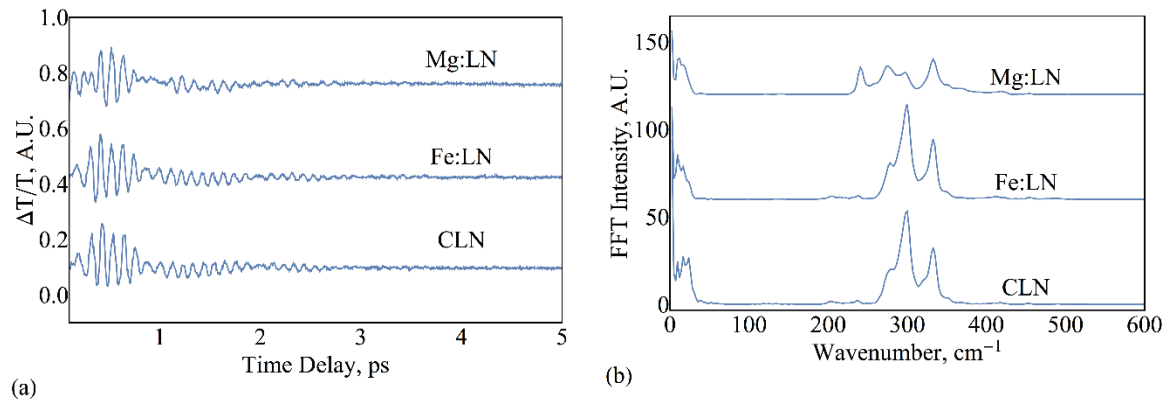
(b) FFTs associated with each scan.

FIG 7. Observation of the effects of doping on lithium niobate samples. Each sample was Z-cut with pump polarization in the X-direction. The graphs show (a) the time-resolved transmission change for CLN and two types of doping and (b) FFTs for each of these scans.
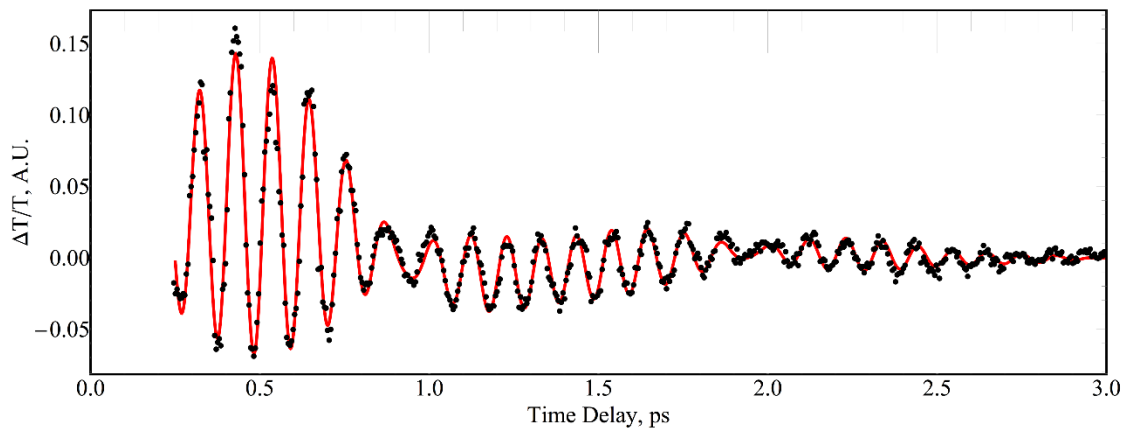

FIG 8. Fit to the Z-cut CLN scan with pump polarization in the X-direction. The fit function is a superposition of decaying sinusoidal functions. In the case of this fit, there are four frequencies used to recreate the scan. The fit parameters for each of the Z-cut scans are shown in Table I.